Organic Electronics 15 (2014) 1324–1337

Contents lists available at ScienceDirect

Organic Electronics

journal homepage: www.elsevier.com/locate/orgel

Stepwise co-sensitization as a useful tool for enhancement of power conversion efficiency of dye-sensitized solar cells: The case of an unsymmetrical porphyrin dyad and a metal-free organic dye

G.D. Sharma [a,*], G.E. Zervaki [b], P.A. Angaridis [b], A. Vatikioti [b], K.S.V. Gupta [c], T. Gayathri [c], P. Nagarjuna [c], Surya Prakash Singh [c,*], M. Chandrasekharam [c], Ajita Banthiya [c], K. Bhanuprakash [c], A. Petrou [b], A.G. Coutsolelos [b,*]

[a] R & D Center for Engineering and Science, JEC Group of Colleges, JEC Campus, Kukas, Jaipur 303101, Rajasthan, India
[b] Laboratory of Bioinorganic Chemistry, Department of Chemistry, University of Crete, Voutes Campus, P.O. Box 2208, 71003 Heraklion, Crete, Greece
[c] Inorganic and Physical Chemistry Division, CSIR-Indian Institute of Chemical Technology, Tarnaka, Hyderabad 500 007, India

ARTICLE INFO

Article history:
Received 10 December 2013
Received in revised form 21 March 2014
Accepted 21 March 2014
Available online 5 April 2014

Keywords:
Co-sensitization
Dye sensitized solar cells
Formic acid treated TiO_2 photoanode
Power conversion efficiency

ABSTRACT

A tertiary arylamine compound (**DC**), which contains a terminal cyano-acetic group in one of its aryl groups, and an unsymmetrical porphyrin dyad of the type Zn[Porph]-L-H_2[Porph] (**ZnP-H_2P**), where Zn[Porph] and H_2[Porph] are metallated and free-base porphyrin units, respectively, and L is a bridging triazine group functionalized with a glycine moiety, and were synthesized and used for the fabrication of co-sensitized dye-sensitized solar cells (DSSCs). The photophysical and electronic properties of the two compounds revealed spectral absorption features and frontier orbital energy levels that are appropriate for use in DSSCs. Following a stepwise co-sensitization procedure, by immersing the TiO_2 electrode in separate solutions of the dyes in different sequence, two co-sensitized solar cells were obtained: devices **C** (**ZnP-H_2P/DC**) and **D** (**DC/ZnP-H_2P**).The two solar cells were found to exhibit power conversion efficiencies (PCEs) of 6.16% and 4.80%, respectively. The higher PCE value of device **C**, which is also higher than that of the individually sensitized devices based on the **ZnP-H_2P** and **DC** dyes, is attributed to enhanced photovoltaic parameters, i.e. short circuit current (J_{sc} = 11.72 mA/cm^2), open circuit voltage (V_{oc} = 0.72 V), fill factor (FF = 0.73), as it is revealed by photovoltaic measurements (J–V curves) and by incident photon to current conversion efficiency (IPCE) spectra of the devices, and to a higher total dye loading. The overall performance of device **C** was further improved up to 7.68% (with J_{sc} = 13.45 mA/cm^2, V_{oc} = 0.76 V, and FF = 0.75), when a formic acid treated TiO_2 **ZnP-H_2P** co-sensitized photoanode was employed (device **E**). The increased PCE value of device **E** has been attributed to an enhanced J_{sc} value (=13.45 mA/cm^2), which resulted from an increased dye loading, and an enhanced V_{oc} value (=0.76 V), attributed to an upward shift and increased of electron density in the TiO_2 CB. Furthermore, dark current and electrochemical impedance spectra (EIS) of device **E** revealed an enhanced electron transport rate in the formic acid treated TiO_2 photoanode, suppressed electron recombination at the photoanode/dye/electrolyte interface, as well as shorter electron transport time (τ_d), and longer electron lifetime (τ_e).

* Corresponding authors. Tel.: +30 2810545045 (A.G. Coutsolelos).
E-mail addresses: gdsharma273@gmail.com (G.D. Sharma), spsingh@iict.res.in (S.P. Singh), coutsole@chemistry.uoc.gr (A.G. Coutsolelos).

http://dx.doi.org/10.1016/j.orgel.2014.03.033
1566-1199/

1. Introduction

Dye-sensitized solar cells (DSSCs) is an emerging solar technology that is considered to be an alternative to the conventional first and second generation photovoltaic devices, due to their simple structure, low cost, ease of fabrication, and high power conversion efficiencies (PCEs). Since the ground-breaking report of O'Regan and Grätzel in 1991 [1], on the fabrication of an efficient solar cell device based on a TiO_2 electrode (anode) sensitized to visible light by an adsorbed poly-pyridyl ruthenium dye in the presence of an I^-/I_3^- redox electrolyte, extensive research, both in theoretical and experimental level, has been conducted in the area of DSSCs in order to understand the processes in a DSSC device, and to improve their efficiency, durability and processability [2–6].

Among the various factors that influence the efficiency of DSSCs, the type of sensitizer is of great importance, since it is responsible for fundamental processes in DSSCs, such as light absorption, injection of electrons into the TiO_2 conduction band (CB), regeneration by the redox electrolyte, and electron recombination. Specifically, the light harvesting efficiency of a DSSC, which is related to the absorption profile of the sensitizer, plays a significant role in the generated photocurrent. An ideal sensitizer should strongly absorb light in a wide spectral region. In an effort to increase the light harvesting efficiency in DSSCs, a variety of different types of sensitizers has been utilized, which include metal–organic, organic, and porphyrin dyes. The most efficient dyes that have been reported to date are based on ruthenium polypyridyl complexes, which convert solar energy to electricity with an efficiency of 11% [7]. However, despite the fact that they exhibit a wide absorption range from visible to near infrared regions [8], their success has been mostly attributed to the appropriately positioned energy levels of their frontier molecular orbitals with respect to the TiO_2 CB, which result in electron injection that is faster than recombination. In addition, their high cost and environmental concerns limit their wide commercial application.

An effective approach to extend the light harvesting efficiency of DSSCs is to design and synthesize molecular sensitizers that efficiently absorb sunlight from the visible to the near IR region so as to exploit photons of longer wavelengths. For example, it has been estimated that by utilizing a molecular sensitizer that absorbs ~80% of incident solar light in the 350–900 nm region (in a DSSC with I^-/I_3^- redox electrolyte), an overall efficiency of 15% should be expected [9]. However, the synthesis of compounds that absorb light over such a wide spectral range (panchromatic sensitizers) is very difficult and expensive, as it may involve complex, reaction and purification procedures. Furthermore, molecular sensitizers with very wide absorption profiles may not be able to provide efficient electron injection into the TiO_2 CB. Due to the fact that they exhibit small band gaps, their LUMO energy levels might be so close to the TiO_2 CB, that the there would not be sufficient thermodynamic driving force for electron injection.

A second approach for extending the light harvesting efficiency of DSSCs involves the co-sensitization of the TiO_2 film of the photoanode with two or more molecular sensitizers that exhibit strong and complementary absorption profiles [10,19]. Various combinations of dyes have been used for DSSC co-sensitization, resulting in enhanced photovoltaic performance relative to the systems sensitized by single dyes. These include ruthenium (II) complexes with organic dyes [11,12] and metal free organic dyes [13,14], and phthalocyanines with organic dyes [15]. Porphyrins, due to their strong and moderate absorptions in the regions of 400–500 nm (Soret band) and 550–700 nm (Q band), respectively, are considered to be ideal candidates for improvement of photovoltaic performance via co-sensitization [16,17]. When they are co-adsorbed on TiO_2 films with other dyes with a complementary absorption profile, panchromatic sensitization can be achieved, leading to significant improvement of the solar cell efficiencies [18–20]. In a particular case, co-sensitization of an appropriately functionalized "push–pull" zinc-metallated porphyrin (with a donor-π-acceptor, D-π-A, architecture) in combination with a metal-free organic dye raised the overall efficiency of DSSCs to the record value of 12.3% [21]. A similar, but not so effective method for improvement of the photovoltaic characteristics of DSSCs is the co-adsorption of molecules, such as chenodeoxycholic acid (CDCA), that reduce the aggregation of the sensitizer on the TiO_2 surface. The formation of dye aggregates significantly decreases the efficiency of electron injection, and causes an adverse effect on the overall performance of DSSCs. However, since co-adsorbents are generally used in large amounts, their crucial drawback is that they occupy large section of the TiO_2 surface without contributing to light absorption [22].

Continuing our studies on sensitization of solar cells porphyrin dyes, we recently reported the synthesis of an unsymmetrical porphyrin dyad of the type Zn[Porph]-L-H_2-[Porph], **ZnP-H_2P**, where Zn[Porph] and H_2[Porph] are metallated and free-base porphyrin units, respectively, and L is a bridging triazine group functionalized with a glycine moiety (Scheme 1) [23]. The **ZnP-H_2P** based solar cell device resulted in a relatively low PCE value of 4.46%, apparently due to the lack of absorption in the 450–550 nm region. In order to improve the light harvesting efficiency of that DSSC, we synthesized a metal-free organic dye, i.e. a tertiary arylamine compound, which contains a cyano-acetic group in one of its aryl groups and a D-π-A architecture (**DC**) (Scheme 1b), and used it as a co-sensitizer along with the **ZnP-H_2P**. By immersing the TiO_2 photoanode successively in solutions of the **ZnP-H_2P** and **DC** dyes, the PCE value of the resulting **ZnP-H_2P/DC** co-sensitized device was improved (from 4.56% for the **ZnP-H_2P**-sensitized solar cell and 4.06% for the **DC**-sensitized solar cell) to 6.16%. The overall efficiency of the co-sensitized solar cell was further improved up to 7.68%, by utilizing a formic acid treated TiO_2 photoanode.

2. Experimental methods

2.1. General methods and materials

All manipulations were carried out using standard Schlenk techniques under nitrogen atmosphere. All chemicals and solvents were purchased from usual commercial

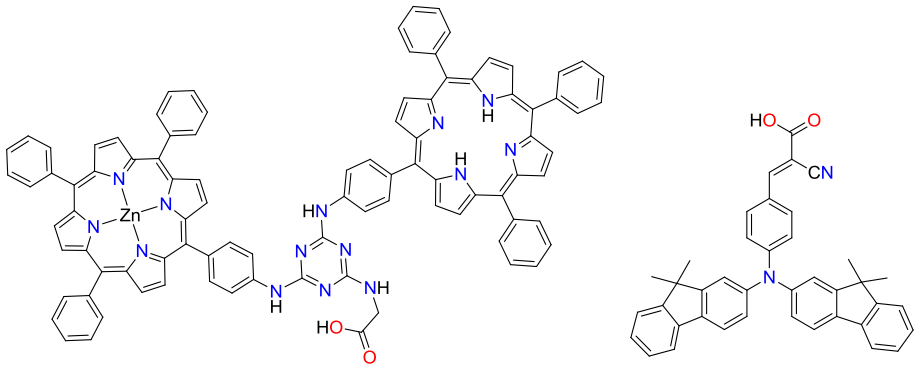

Scheme 1. Structures of porphyrin dyad **ZnP-H_2P** and metal-free organic dye **DC**.

sources and used as received, unless otherwise stated. Solvents were distilled from appropriate reagents.

Porphyrin dyad **ZnP-H_2P**, namely 5-{4-[3-(5-(4-aminophenyl)-10,15,20-triphenyl-porphyrinato)-5-glycine-triazinyl]-aminophenyl}-10,15,20-triphenyl-porphyrin zinc, was prepared from cyanuric chloride by adding successively 5-(4-aminophenyl)-10,15,20-triphenyl-porphyrinato zinc Zn[TPP-NH_2],5-(4-aminophenyl)-10,15,20-triphenyl-porphyrin H_2[TPP-NH_2] (prepared according to literature procedures [24]), and glycine methyl ester hydrochloride in dry THF, in the presence of DIPEA, followed by basic hydrolysis with KOH, as described in our earlier communication [21]. Satisfactory analytical and spectroscopic characteristics were obtained.

2.2. Synthesis

2.2.1. Metal-free organic dye ***DC***

To a solution of 4-(bis (9,9-dimethyl-9H-fluoren-3-yl)amino) benzaldehyde (0.100 g, 0.197 mmol) and cyanoacetic acid (0.025 g, 0.295 mmol) in acetic acid (5 mL), ammonium acetate (10% mol) was added, under nitrogen atmosphere. The reaction mixture was refluxed for 12 h and then cooled to room temperature. Addition of ice-cold water resulted in the precipitation of a solid, which was filtered-off, washed with hexane (30 ml) and dried under vacuum. The product was isolated as red solid in 76% yield.

^{1}H NMR (300 MHz, $CDCl_3$):δ(ppm) 8.15(*s*, 1H), 7.90–7.93(*m*, 2H), 7.68–7.70(*m*, 4H), 7.30–7.43(*m*, 8H), 7.11–7.22(*m*, 4H), 1.43(*s*, 12H).

^{13}C NMR (75 MHz, $CDCl_3$): δ(ppm): 155.49, 154.98, 153.66, 153.05, 144.87, 138.36, 136.73, 133.64, 127.19, 127.10, 127.04, 126.86, 126.37, 125.09, 124.16, 123.17, 122.55, 120.99, 120.52, 119.85, 119.68,119.59,119.51,46.95, 26.96. IR (KBr, cm^{-1}): 3442, 2956, 2924, 2853, 2215, 1738, 1577, 1506, 1448, 1348, 1313, 1277, 1217, 1181, 829, 736. MS(ESI) *m*/*z*: 595 $(M + Na)^+$.

2.3. Characterization methods

^{1}H and ^{13}C NMR spectra were recorded on Bruker DPX-300 MHz spectrometer as solutions in deuterated solvents by using the solvent peak as the internal standard. Low resolution mass spectrometry was performed using LCQ ion trap mass spectrometer (Thermo Fisher, Sanjose, CA, USA) equipped with an ESI source. FTIR spectra were recorded on a Perkin Elmer 16PC FTIR spectrometer. UV–vis absorption spectra were measured on a Shimadzu UV-1700 spectrophotometer using 10 mm path-length cuvettes. Cyclic voltammetry experiments were carried out at room temperature using an AutoLab PGSTAT20 potentiostat and appropriate routines available in the operating software (GPES, version 4.9). Measurements were carried out in freshly distilled and deoxygenated CH_2Cl_2, at a rate of 100 mV/s with a solute concentration of 1.0 mM in the presence of tetrabutylammonium hexafluorophosphate (0.1 M) as supporting electrolyte. A three-electrode cell setup was used with a platinum working electrode, a saturated calomel (SCE) reference electrode, and a platinum wire as counter electrode.

2.4. Computational methods

Quantum chemical calculation were performed within the frame work of density functional theory (DFT) [25], using the GAUSSIAN 09 program suite [26]. Gas phase geometry optimizations were carried out by employing Becke three parameter exchange in conjunction with Lee–Yang–Parr correlation functional (B3LYP) [27,28], and the 6-311G (d,p) basis set. The optimized minimum-energy structures were verified as stationary points on the potential energy surface by vibrational frequency analysis calculation. Computed structures and molecular orbitals were visualized and analyzed by Gauss View software [29].

2.5. Preparation of TiO_2 electrodes and DSSCs

The DSSCs were fabricated using electrodes based on fluorine doped tin oxide (FTO) glass substrates, which were pre-cleaned by sonication in decon 90, distilled water, isopropanol (*i*-PrOH), ethanol (EtOH), and dried in air.

The working electrodes were prepared by firstly forming a blocking layer of 0.2 M titanium di-isopropoxide bis(acetylacetonate) in *i*-PrOH by spray pyrolysis on pre-cleaned FTO coated glass substrates, followed by the

deposition of nano-crystalline layer of TiO_2 using doctor blade technique, by employing a dye sol TiO_2 paste (DSL 18NR-T). The TiO_2 coated electrodes were heated at 500 °C for 30 min, and then cooled at room temperature. For the preparation of the formic acid treated TiO_2 photoanode, the TiO_2 electrode was treated with a 0.05 M formic acid solution in EtOH for 1 h, washed with EtOH, and finally dried in ambient conditions. The thicknesses of the TiO_2 electrodes were measured using a thin film thickness measurement system and they were found to be in the range of 10–12 μm. The dye solutions were prepared as follows: 3×10^{-4} M **ZnP-H_2P** in $CHCl_3$/EtOH (1/1 volume ratio) and 5×10^{-4} M **DC** in THF. Photoanodes sensitized with single dyes were prepared by immersing the TiO_2 electrode into the respective solutions of dyes **ZnP-H_2P** and **DC** for 4 h, rinsed with EtOH and dried in air. For the co-sensitization, the pure TiO_2 and formic acid treated TiO_2 photoanodes were dipped into the solution of the first dye for 4 h, rinsed with EtOH, and then dipped into the solution of the second dye for 4 h, rinsed with EtOH, and dried in air. The counter electrode was prepared by spin coating a H_2PtCl_4 solution (2 mg in 1 mL of *i*-PrOH) onto a pre-cleaned FTO coated glass substrate and then heating at 450 °C for 15 min in air. The sensitized working electrode was assembled with the Pt coated FTO electrode into a sandwich type cell and sealed with a hot-melt polymer surlyn.

To complete the DSSC fabrication, the electrolyte solution containing LiI (0.05 M), I_2 (0.03 M), 1 methyl-3-n-propylimidazolium iodide (0.6 M) and 0.5 M *tert*-butylpyridine in a mixture of acetonitrile and valeronitrile (85:15 volume ratio) was introduced into the space between the two electrodes through the drilled hole on Pt coated FTO by vacuum backfilling.

2.6. Photovoltaic measurements

The current–voltage (*J*–*V*) characteristics of the DSSCs, in dark and under illumination, were measured using a computer controlled Keithley source meter (model 2601 A). A solar simulator TS space system class AAA was used to give an irradiance of 100 mW/cm^2 at the surface of the device under standard air mass (AM1.5). The incident photon to current efficiency (IPCE) spectra of the DSSCs was measured using a Bentham IPCE system (TMc 300 monochromator computer controlled). The Electrochemical impedance spectra (EIS), in dark and under illumination, were recorded using a CHN electrochemical workstation, by applying a dc bias equivalent to the open circuit voltage of the DSSC, in the frequency range of 0.1–10^5 Hz.

3. Results and discussion

3.1. Molecular structures and syntheses of dyes

As shown in 1, porphyrin dyad **ZnP-H_2P** consists of two *meso*-phenyl-substituted porphyrin units ZnP and H_2P (where ZnP and H_2P are the zinc-metallated and free-base forms of 5-(4-aminophenyl)-10,15,20-triphenylporphyrin, respectively), which are covalently bridged by a 1,3,5-triazine group. **ZnP-H_2P** is also functionalized at the third position of the triazine ring by a glycine moiety with a terminal carboxylic acid group, which can be used as binding group for anchoring onto the TiO_2 surface of DSSC electrodes. The synthesis of **ZnP-H_2P** (described in our earlier report [17]) was achieved by stepwise amination reactions of cyanuric chloride with successive additions of Zn[TPP-NH_2],H_2[TPP-NH_2], and glycine methyl ester hydrochloride in THF, in the presence of DIPEA, followed by basic hydrolysis with KOH.

Metal-free organic dye **DC** (Scheme 1) is a tertiary amine consisting of two dimethylfluorenyl groups and a phenyl cyanoacetic group. Taking into account that the former are two electron donating groups (A), while the latter is an electron accepting group (A), **DC** can be considered as having the donor–acceptor, D–A, architecture. **DC** was synthesized following the stepwise procedure illustrated in Scheme 2. The intermediate 4-(bis(9,9-dimethyl-9H-fluoren-3-yl)amino) benzaldehyde was synthesized according to previously published procedures in 90% yield [30]. In the final step, the aldehyde was converted into the **DC** dye through a Knoevenagel reaction by treating an acetic acid solution of the aldehyde with cyanoacetic acid in 110 °C for 12 h, using a catalytic amount of ammonium acetate. ^{1}H and ^{13}C NMR, and ESI measurements confirmed the identity of the resulting compound.

3.2. Photophysical properties

The UV–vis absorption spectra of the porphyrin dyad **ZnP-H_2P** and the metal-free organic dye **DC** in solutions (0.3 mM in $CHCl_3$/EtOH = 1/1) are shown in Fig. 1 (black and grey color[1] lines, respectively). **ZnP-H_2P** exhibits the typical porphyrin absorption bands, with an intense Soret band in the 400–440 nm range and two moderate absorption bands in the 520–600 nm range. The broadening and splitting of the Soret band can be attributed to a strong exciton coupling between porphyrin units of different dyads in their exited states or to a lowering of molecular symmetry [31]. In case of **DC**, the UV–vis absorption spectrum displays a broad and intense absorption band centered at 456 nm, with a molar extinction coefficient of 34,500 M^{-1} cm^{-1}, which could be ascribed to an intramolecular charge transfer (ICT) between the bis-(fluoren-3-yl)amino group (donor) and the cyanoacetic group (acceptor) of the molecule.

In Fig. 2, the UV–vis absorption spectra of **ZnP-H_2P** and **DC** adsorbed onto the surface of TiO_2 films of 10–12 thickness are depicted (black and red color lines, respectively). They display similar absorption features with the corresponding spectra of the dyes in solution, but these are broader and redshifted. The UV–vis spectrum of the co-sensitized TiO_2 film with both dyes**ZnP-H_2P** and **DC** (blue color line) exhibits enhanced, broad light absorption in the 400–650 nm region, compared with the spectra of the individually sensitized TiO_2 films. In addition, in the co-sensitized TiO_2 film, the absorption band that corresponds to the Soret band of **ZnP-H_2P** is broader. This suggests that

[1] For interpretation of color in Fig. 1, the reader is referred to the web version of this article.

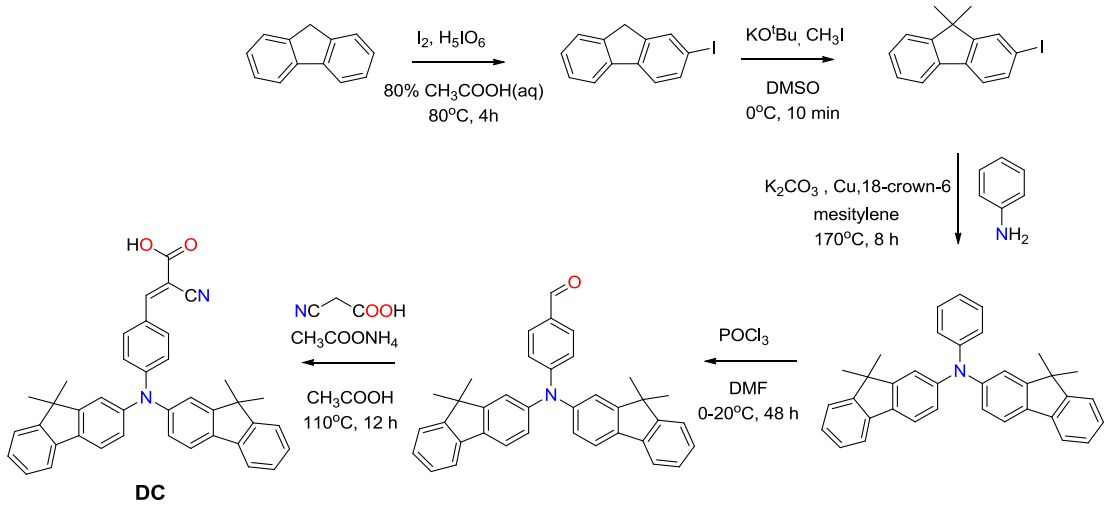

Scheme 2. Synthesis of metal free dye **DC**.

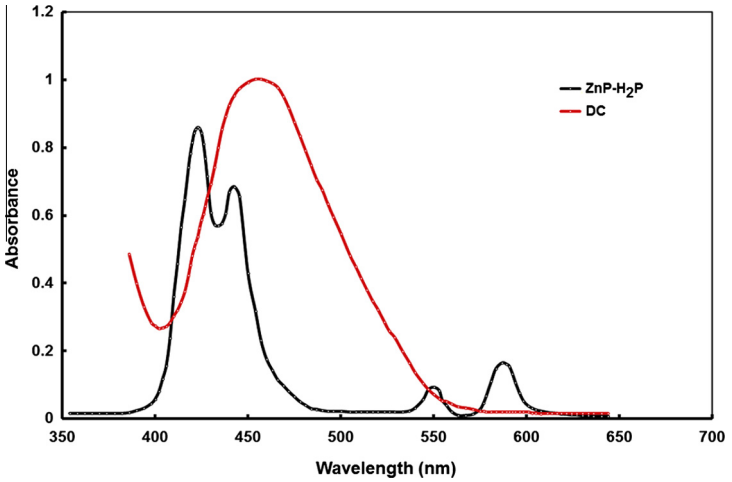

Fig. 1. Normalized UV–vis absorption spectra of **ZnP-H_2P** and **DC** in $CHCl_3$/EtOH (=1/1) solution.

the co-adsorption of **DC** causes a change of the orientation of the molecules of **ZnP-H_2P** adsorbed on the TiO_2 surface, that results in decrease of their aggregation, as a consequence of steric repulsions with the co-adsorbed **DC** molecules [16,32].

3.3. Electrochemical properties

The redox properties of the porphyrin dyad **ZnP-H_2P** and the metal-free organic dye **DC** were investigated by cyclic voltammetry measurements, in order to evaluate if there are favorable energy offsets of the dyes with respect to the TiO_2 film and the electrolyte.

Porphyrin dyad **ZnP-H_2P** exhibits a quasi-reversible oxidation at E^1_{ox} = +1.16 V *vs* NHE and a quasi-reversible reduction at E^1_{red} = −0.89 V *vs* NHE [21]. Metal-free organic dye **DC** exhibits analogous oxidation and reduction processes at E^1_{ox} = +0.80 V *vs* NHE and E^1_{red} = −1.25 V *vs* NHE. For efficient electron injection from the photoexcited dyes into the TiO_2 CB, the E^1_{red} values of both dyes (which correspond to their lowest unoccupied molecular orbital, LUMO, energy levels), should be higher than the TiO_2 CB edge (−0.5 V *vs* NHE). Furthermore, for efficient dye regeneration (after dye photo-excitation and electron injection), the E^1_{ox} values of the dyes (which correspond to their highest occupied molecular orbital, HOMO, energy levels), should be lower than the redox potential of I^-/I_3^- couple (+0.4 V vs NHE). As shown in Fig. 3, in which the E^1_{ox} and E^1_{red} values of the dyes **ZnP-H_2P**, **DC**, together with the potentials of the TiO_2 CB edge and the redox potential of I^-/I_3^- couple, are depicted, both criteria are met, and, therefore, there is sufficient thermodynamic force for electron injection and regeneration of the photo-oxidized dyes [33].

3.4. Theoretical calculations

To get a better insight into the electronic structures of the dyes**ZnP-H_2P** and **DC**, DFT calculations at the B3LYP/6-311G(d,p) level of theory were employed. The results

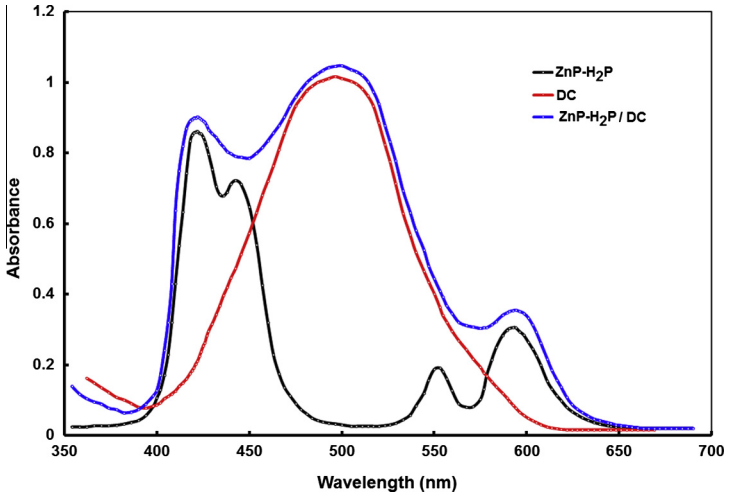

Fig. 2. Normalized UV–vis absorption spectra of **ZnP-H_2P**, **DC** and **ZnP-HP/DC** adsorbed onto TiO_2 films.

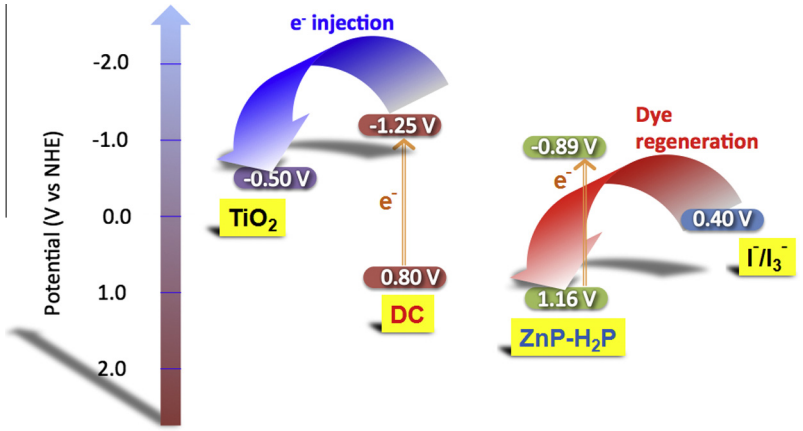

Fig. 3. Electrochemical potential diagram of **ZnP-H_2P**, **DC**, TiO_2 CB edge, and I^-/I_3^- couple, showing the feasibility of electron injection and dye regeneration processes.

of the calculations for **ZnP-H_2P** [21], revealed a "butterfly-like" molecular geometry, with the porphyrin units being in an almost perpendicular orientation with respect to the triazine ring. The HOMO and LUMO electron densities were found to be localized on the porphyrin units and not on the carboxylic acid anchoring group of the glycine moiety.

The ground state geometry optimized structure of **DC** revealed a distorted trigonal pyramidal molecular geometry. As shown from the electronic density distributions of the frontier orbitals (Fig. 4), the HOMO is delocalized over the entire molecule, but in the LUMO most of the electronic density is localized over the cyanoacetic anchoring group. According to the Franck Condon principle, the overlap of the HOMO and LUMO levels by the π-bridging nitrogen atom enhances the electronic transition dipole moments between the vibrational energy levels. This suggests that the strong intramolecular charge transfer (ICT) nature of **DC** upon illumination would result in efficient electron injection from the excited dye to TiO_2 CB.

The HOMO–LUMO band gaps of both dyes **ZnP-H_2P** and **DC**, as estimated by DFT calculations, are in good agreement with those obtained from the electrochemically observed oxidation E_{ox} and reduction potentials E_{red} of the respective compounds.

3.5. Photovoltaic properties

3.5.1. Photovoltaic properties of co-sensitized DSSCs

For the fabrication of the co-sensitized DSSCs, a stepwise co-sensitization procedure was followed, by sequentially immersing the TiO_2 electrode (with thickness of 10–12 μm) in separate solutions of the **ZnP-H_2P** and **DC** dyes [34]. In one case, the TiO_2 photoanode was firstly immersed into the **ZnP-H_2P** solution and secondly in the **DC** solution resulting in device **C** (or device **ZnP-H_2P**/**DC**), while in another case, the reverse order was followed, i.e. first in the **DC** and then in the **ZnP-H_2P** solution, resulting in device **D** (or device **DC**/**ZnP-H_2P**). The optimum soaking time for the TiO_2 photoanode film in each one of the dye

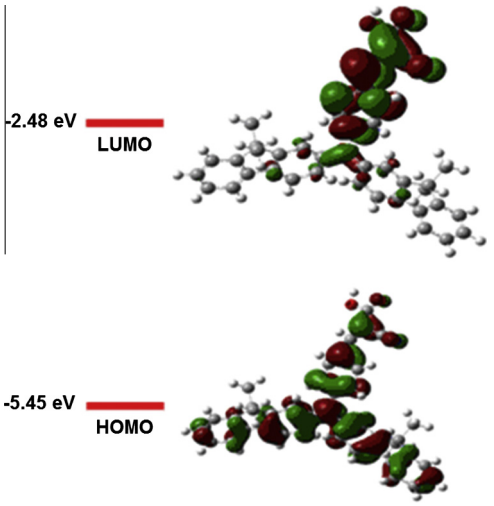

Fig. 4. The HOMO and LUMO energy levels of **DC** and their corresponding electronic density distributions.

solutions was found to be 6 h. For comparison purposes, solar cells sensitized by the individual dyes **ZnP-H$_2$P** (device **A**) and **DC** (device **B**), were also fabricated, under the same experimental conditions.

The current–voltage (*J*–*V*) characteristics, under illumination (AM1.5, 100 mW/cm^2), of the solar cell devices **A** and **B**are shown in Fig. 5 (black and red color lines, respectively), while those of the solar cell devices **C** and **D** are shown in Fig. 6 (black and red color lines, respectively). The photovoltaic cell parameters of all devices, i.e. short circuit current J_{sc}, open circuit voltage V_{oc}, fill factor *FF* and overall power conversion efficiency PCE, are summarized in Table 1. The individually sensitized devices **A** and **B** were found to exhibit PCE values of 4.56% (with J_{sc} = 10.18 mA/cm^2, V_{oc} = 0.66 V, and *FF* = 0.68), and 4.45% (with J_{sc} = 9.76 mA/cm^2, V_{oc} = 0.68, and *FF* = 0.67), respectively, while the co-sensitized solar cell devices **C** and **D** showed PCE values of 6.16% (with J_{sc} = 11.72 mA/cm^2, V_{oc} = 0.72 V, and *FF* = 0.73), and 4.80% (with J_{sc} = 10.08 - mA/cm^2, V_{oc} = 0.68 V, and *FF* = 0.70), respectively.

The higher PCE value of the co-sensitized device **C** (or device **ZnP-H$_2$P**/**DC**), compared with to the individually sensitized devices **A** and **B**, is attributed to the enhanced photovoltaic parameters J_{sc}, V_{oc} and *FF*. Particularly, the enhanced J_{sc} value is ascribed to the enhanced IPCE response of the cell, since they are related by the equation

$$J_{SC} = \int e\phi_{ph,AM1.5G}(\lambda)IPCE(\lambda)d\lambda \quad (1)$$

where *e* is the elementary charge and $\varphi_{ph,AM1.5}$ is the photon flux at AM1.5 [2,35]. The IPCE response of the solar cell can be expressed by the equation

$$IPCE(\lambda) = LHE(\lambda)\eta_{inj}(\lambda)\eta_{cc}(\lambda) = (1 - 10^{-A})\eta_{inj}(\lambda)\eta_{cc} \quad (2)$$

where *LHE* is the light harvesting efficiency, η_{inj} is the electron injection efficiency, η_{cc} is the charge collection efficiency, and A is the absorbance of the photoanode. Among the three factors, LHE plays a very important role, and it depends on the absorption profiles of the co-sensitizing dyes **ZnP-H$_2$P** and **DC** (their molar absorption coefficients), the relative amounts of dyes adsorbed onto the TiO_2 surface (dye loadings) of the photoanode, and the optical path length within the electrode. In addition, as discussed above, since the LUMO energy levels of both **ZnP-H$_2$P** and **DC** lie above the TiO_2 CB edge, the electron injection from the photo-excited states of dyes to the TiO_2 CB is thermodynamically favorable.

As shown in the UV–vis absorption spectra of the dyes **ZnP-H$_2$P**, **DC**, and **ZnP-H$_2$P**/**DC** adsorbed onto TiO_2 films (Fig. 2), the **DC** sensitized film exhibits very strong absorption in the 460–530 nm range, where the absorption of the **ZnP-H$_2$P** sensitized film is weak. Hence, the absorption spectrum of the **ZnP-H$_2$P**/**DC** film exhibits an extended absorption profile with panchromatic features, which can lead to an increased LHE, and enhanced IPCE response for the co-sensitized solar cell device **C** in the wide range of 370–670 nm, with the highest IPCE value of 70% at ~440 nm (Fig. 7, light blue color line).Comparison of the

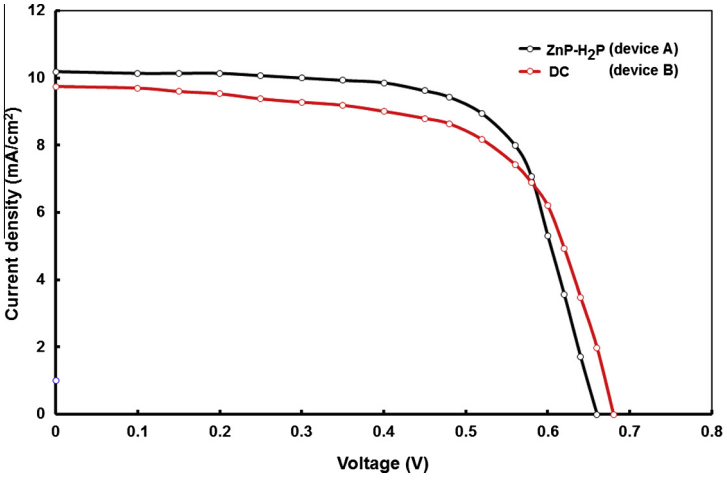

Fig. 5. Current–voltage (*J*–*V*) characteristics, under illumination, of devices **A** and **B**.

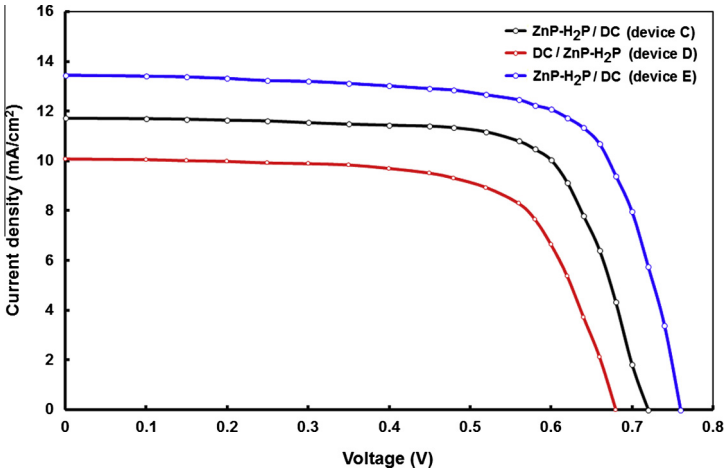

Fig. 6. Current–voltage (J–V) characteristics, under illumination, of co-sensitized devices **C**, **D** and **E**.

Table 1
Photovoltaic parameters, i.e. short circuit current (J_{sc}), open circuit voltage (V_{oc}), fill factor (FF), and photo conversion efficiency (PCE), of devices **A**, **B**, **C**, **D** and **E**.

Device	J_{sc} (mA/cm^2)	V_{oc} (V)	*FF*	PCE (%)
A	10.18	0.68	0.68	4.56
B	9.05	0.66	0.66	4.06
C	11.72	0.72	0.73	6.16
D	10.08	0.68	0.70	4.80
E	13.45	0.76	0.75	7.68

IPCE spectra of devices **A**, **B**, and **C** in the wavelength region below 500 nm shows that the IPCE response of the co-sensitized device **C** is slightly enhanced. Considering that in this wavelength region appears the Soret band absorption of the porphyrin dyad **ZnP-H$_2$P**, while the metal-free organic dye **DC** does not display any absorption, co-sensitization by **DC** does not contribute to the observed enhanced photocurrent generation, and the LHE and charge collection efficiency of device **C** should be the same as in device **A**. The observed IPCE enhancement may be attributed to the improved charge collection efficiency, which is due to dye **DC** impeding the electron leakage by an increased molecular surface coverage upon co-sensitization.

The dye loading values of the co-sensitized solar cell device **C**, as well as those of the individually sensitized solar cell devices **A** and **B**, was determined. For device **C**, the amounts of **ZnP-H$_2$P** and **DC** adsorbed onto the TiO_2 photoanode were found to be 1.9×10^{-7} and 1.8×10^{-7} mol/cm^2 respectively, while for devices **A** and **B**, they were found to be 2.1×10^{-7} and 3.4×10^{-7} mol/cm^2, respectively. The total dye loading in the co-sensitized device **C** is higher than the dye loadings in the individually sensitized solar cell devices **A** and **B**. Consequently, device **C** exhibits an increased LHE value, and enhanced IPCE response, and hence to a higher PCE value. This may be understood in the context of the difference of the molecular sizes of **ZnP-H$_2$P** and **DC**. Upon adsorption of the larger size **ZnP-H$_2$P** molecules onto the TiO_2 surface in the first

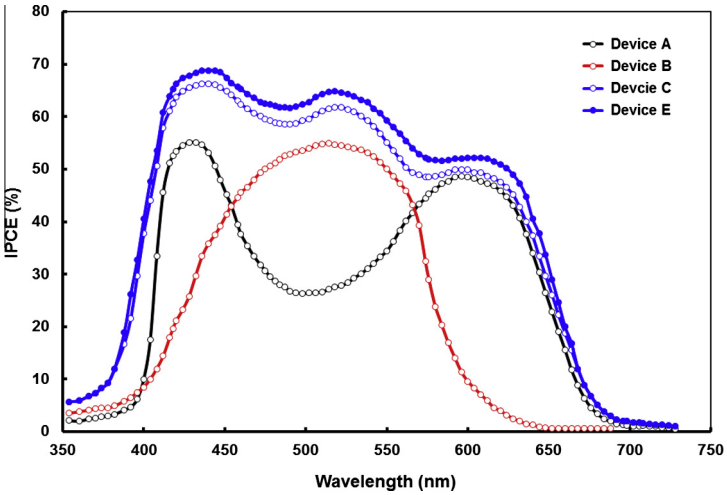

Fig. 7. Incident photon to current conversion efficiency (IPCE) spectra of devices**A**, **B**, **C**, and **E**.

step of co-sensitization, the smaller size molecules of **DC** are adsorbed onto the TiO_2 film in such a way that they fill the gaps between the porphyrin dyad molecules. As a result, an increased total dye loading is obtained. The smaller molecular size of **DC** is also the reason for the higher **DC** loading in the individually sensitized device **B** than the **ZnP-H$_2$P** loading in device **A**, since a larger number of molecules can be accommodated in the same TiO_2 surface. However, in device **C**, the **ZnP-H$_2$P** loading was found to be higher than the **DC** loading. This is a result of the stepwise co-sensitization procedure. In the **ZnP-H$_2$P** saturated TiO_2 film, there is only a small surface area available for binding of **DC**. In addition, the dye loading of **ZnP-H$_2$P** in the co-sensitized device **C** was found to be lower than that in the individually sensitized device **A** (1.9×10^{-7} vs 2.1×10^{-7} mol/cm^2, respectively). This may be attributed to a partial detachment of **ZnP-H$_2$P** molecules from the TiO_2 surface, after immersing the **ZnP-H$_2$P** sensitized TiO_2 film into the **DC** solution, in the second step of the co-sensitization procedure. The **DC** molecules, due to the presence of two anchoring groups, the carboxylic acid and the cyano group in their structures [12,36], exhibit a more effective binding capacity to the TiO_2 surface, relative to the **ZnP-H$_2$P** molecules, which contain one carboxylic acid anchoring group, and therefore they replace some of the already bound **ZnP-H$_2$P** molecules.

In case of co-sensitized device **D** (or device **DC**/**ZnP-H$_2$P**), the PCE value was found to be lower than that of co-sensitized device **C**, and marginally higher than those of the individually sensitized solar cell devices **A** and **B**. This can be attributed to the lower photovoltaic parameter values J_{sc}, V_{oc} and *FF* of the device (Table 1 and Fig. 6).

The IPCE response of device **D** in the 570–630 nm region is higher than that for device **C**, resulting in an enhanced photocurrent generation. Since in this wavelength region appears the Q band absorption of the porphyrin dyad **ZnP-H$_2$P** and **DC** does not absorb light, the improved IPCE response is a result of the enhanced LHE value of the co-sensitized solar cell due to **ZnP-H$_2$P** co-sensitization. Upon immersing the **DC** saturated TiO_2 into the solution of **ZnP-H$_2$P**, a small number of **DC** molecules adsorbed onto the TiO_2 surface are replaced by **ZnP-H$_2$P** molecules.

The overall amount of dye adsorbed onto the TiO_2 photoanode of device **D** is lower than that for device **C**. This can be related to the larger molecular size of **ZnP-H$_2$P** with respect to **DC**. After adsorption of the small size **DC** molecules onto the TiO_2 surface in the first step of co-sensitization, only a small space of the TiO_2 is available for adsorption of the larger size molecules of **ZnP-H$_2$P**. Therefore, a small dye loading of **ZnP-H$_2$P** is obtained. The reduced total dye loading leads to a suppressed LHE value, and a low IPCE response, and hence to a lower PCE value.

3.5.2. Photophysical properties of co-sensitized DSSCs with formic acid treated TiO_2 photoanode

Generally, in order to improve the performance of DSSCs, a number of aspects should be considered. Among them, the mesoporous semiconductor oxide film of the photoanode, e.g. TiO_2, is of great importance, since it supports the sensitizing dye, collects the injected electrons, and leads the electrons to the outer circuit. The important photovoltaic parameters J_{sc}, V_{oc}, and *FF* are related to the physical and electronic properties of the TiO_2 film. Particularly, J_{sc} depends on the amount of dye loading on the TiO_2 surface, the efficiency of the electron injection from the dye into the TiO_2 CB, as well as the charge collection at the counter electrode. V_{oc} is governed by the energy difference between the quasi Fermi level of TiO_2 and the redox potential of electrolyte. Moreover, both J_{sc} and V_{oc} are affected by the recombination kinetics at the TiO_2/dye/electrolyte interface. Therefore, any energy shift of the TiO_2 CB edge affects the molecular and electronic interaction between the sensitizing dye molecules and TiO_2 surface, electrolyte component, and the surface modification of the TiO_2 [37,38], and consequently influences both V_{oc} and J_{sc} of a DSSC, affecting its overall performance.

In an effort to enhance the photocurrent generation and reduce the back electron transfer at TiO_2/dye/electrolyte interface a variety of methods have been employed. These include addition of additives to electrolyte [39], use of a blocking/tunneling layer at TiO_2 surface [40], and surface treatment or modification of the TiO_2 film [41]. A successful method that has been recently introduced is the modification of the interface between the FTO glass substrate and the TiO_2 film, utilizing self-assembled monolayer (SAM) with multiple carboxylic acid functional groups [42,43]. Along these lines, we investigated the effect of treating the TiO_2 photoanode of the co-sensitized solar cell **ZnP-H$_2$P**/**DC** device (device **C**) with formic acid on the overall photovoltaic performance.

The current–voltage (*J*–*V*) characteristics, under illumination (AM1.5, 100 mW/cm^2), of the device with the formic acid treated TiO_2 **ZnP-H$_2$P/DC** co-sensitized photoanode (device **E**) are depicted in Fig. 6 (blue color line) and the corresponding photovoltaic parameters are listed in Table 1. Its PCE value was found to be 7.68%, which is higher than the PCE value of device **C**. This is attributed to the enhancement of the photovoltaic parameters (J_{sc} = 13.45 mA/cm^2, V_{oc} = 0.76 V, and *FF* = 0.75) after the formic acid treatment of the TiO_2 film.

As shown in Fig. 7, the IPCE response of device **E** (blue color line) is enhanced throughout the studied UV–vis wavelength range, compared to the IPCE response of device **C** with the untreated TiO_2 **ZnP-H$_2$P/DC** co-sensitized photoanode (light blue color line). This can be related to the different dye loading values of the two devices. The overall dye loading of device **E** was found to be higher than that of device **C**, resulting in an improved IPCE response and enhanced J_{sc} value.

Furthermore, the V_{oc} value of device **E** was found to be higher relative to device **C**. As mentioned above, the V_{oc} value of a DSSC depends on the energy difference between the quasi Fermi level of TiO_2 and the redox potential of the electrolyte. Since in devices **C** and **E** the same electrolyte was used, the difference between the V_{oc} values is due to the different quasi Fermi levels of TiO_2 in the two photoanodes. The variation of the quasi Fermi levels of TiO_2 (E_F) in the two devices could arises either from a shift of the TiO_2 CB edge (E_{CB}) or from a change in the electron density (n) in the TiO_2 CB, as described in the following expression

$$E_F = E_{CB} + k_B T \ln\left(\frac{n}{N_c}\right) \quad (3)$$

where $k_B T$ is the thermal energy, and N_c is the density of states in the TiO_2 CB [2,44]. In other words, the improved V_{oc} value of the device **E** results from either an upward shift of the TiO_2 CB edge and/or an increase in the electron density in the TiO_2 CB of the formic acid treated photoanode.

In order to get information about the shift of the TiO_2 CB edge in the device **E**, the optical band gaps (E_g^{opt}) of both untreated and formic acid treated TiO_2 **ZnP-H_2P/DC** co-sensitized films were estimated. From the onset absorption edges of the UV–vis spectra of the respective thin films, the optical band gaps of untreated TiO_2 and formic acid treated TiO_2 were calculated to be 3.22 and 3.27 eV, respectively. Assuming that the TiO_2 valence band is −7.4 eV (as reported in literature), the CB edge of the untreated TiO_2 and formic acid treated TiO_2were found to be −4.18 and −4.13 eV, respectively. Based on these values, it can be concluded that the CB edge of the formic acid treated TiO_2 is shifted higher in energy by 0.05 eV, with respect to the untreated TiO_2. This shift may be due to the influence of the lower pH value and surface adsorbent in device **E** [45].

Considering that the upward shift of 0.05 eV of the CB edge of the formic acid treated TiO_2 is small with respect to the relatively large enhancement of 0.08 eV of the V_{oc} value of device **E**, it is conclude that the observed V_{oc} value should also be influenced by the electron density in the TiO_2 CB. The quasi Fermi level of TiO_2 is affected by the change of electron density of the dye sensitized electrode during the illumination. Upon light absorption, electrons from the photo-excited sensitizer are injected into the TiO_2 CB, leading to a significant change of the electron density in the TiO_2 CB that depends on the light harvesting efficiency of the sensitizer and electron injection efficiency at the TiO_2/dye interface. Given that the dye loading is higher for the formic acid treated TiO_2 photoanode, it is expected that the electron density in the CB of the formic acid treated TiO_2 is higher than that with the untreated TiO_2. Hence, the combined effect of the upward shift of the TiO_2 CB edge and the increase of the electron density in the TiO_2 CB leads to an enhanced V_{oc} value for device **E**.

In an effort to gain a better understanding of the enhancement of the V_{oc} value in the solar cell with the formic acid treated TiO_2 **ZnP-H_2P** co-sensitized photoanode, and to investigate the kinetics of the electron transport and recombination processes [46], electrochemical impedance spectra (EIS) of devices **C** and **E** in dark conditions, at a dc bias equivalent to the V_{oc} value, were obtained. The Nyquist plots of the spectra of both solar cells are shown in Fig. 8a (black and red color lines, respectively). In each case, three semicircles are observed, which represent charge transfer resistances at different interfaces of the solar cells. The semicircle in the high frequency range (left side of spectrum) corresponds to the charge transfer impedance at the FTO/TiO_2 interface, the semicircle in the middle frequency range is associated with the charge transfer and recombination impedance at TiO_2/dye/electrolyte interface, while the semicircle in the low frequency range (right side of spectrum) is related to the charge transfer impedance of diffusion processes in the electrolyte [47]. The charge transfer rates at each interface can be compared on the basis of the radii of the semicircles: the larger and smaller semicircle radii represent higher and lower impedances or resistances (R) and, hence, they correspond to slow and fast charge transfer rates, respectively. The charge transfer resistance R_t values and the charge recombination resistance R_{rec} values for devices **C** and **E** are complied in Table 2. Device **E** with the formic acid treated TiO_2 photoanode, compared to device **C** with pristine TiO_2, shows a lower charge transfer resistance R_t value at the FTO/TiO_2 interface (as it is shown from the smaller radius of the high frequency range semicircle), suggesting that the injected electrons from the excited state of dye into TiO_2 CB are easily transported into the FTO electrode. Moreover, the radius of the semicircle that corresponds to the TiO_2/dye/electrolyte for device **E** has a larger radius than that for device **C**, which signifies a higher charge recombination resistance R_{rec} value for the former device. In other words, in device **E** the recombination of the injected electrons into the TiO_2 CB with the electrolyte is suppressed. In total, the reduced charge transfer resistance R_t and the increased charge recombination resistance R_{rec} values for device **E** lead to an improved J_{sc} value (as observed from the J–V characteristics of the devices under illumination).

The electron lifetimes (τ_e) in devices **C** and **E** were calculated from the Bode phase plots of the EIS spectra of the two solar cells (Fig. 8b, black and red color lines, respectively),according to the relationship

$$\tau_e = \frac{1}{2\pi f_{max}} \quad (4)$$

where f_{max} is the frequency at the maximum of the curve in the intermediate frequency region in Bode phase plot, and the results are listed in Table 2. The electron lifetime (τ_e) for the device with the formic acid treated TiO_2 **ZnP-H_2P** co-sensitized photoanode (device **E**) was found to be than for that for the solar cell with the pristine TiO_2 photoanode (device **C**) (38.45 vs 32.64 ms). This difference might be expected, since the adsorbed formic acid molecules onto the TiO_2 surface of device **E** acts as a barrier between the semiconductor and electrolyte and therefore reduce the back electron transfer.

The aforementioned results are also supported by dark current–voltage (J–V) measurements of devices **C** and **E**, which are presented in Fig. 9 (black and red color lines, respectively). In device **E**, compared to device **C**, dark current J is significantly reduced while the onset voltage shifts towards higher voltage values. These results also suggest that in device **E** the back recombination between the electrons in the TiO_2 CB and the electrolyte is suppressed in the upon the formic acid treatment, giving rise to V_{oc} and J_{sc}, resulting in higher overall PCE value.

To get the information about the charge transport mechanism in devices **C** and **E**, their EI spectra under illumination, at a dc bias equivalent to the V_{oc} value, were obtained. In the Nyquist plots of these spectra three semicircles are also observed. The semicircle in the intermedi-

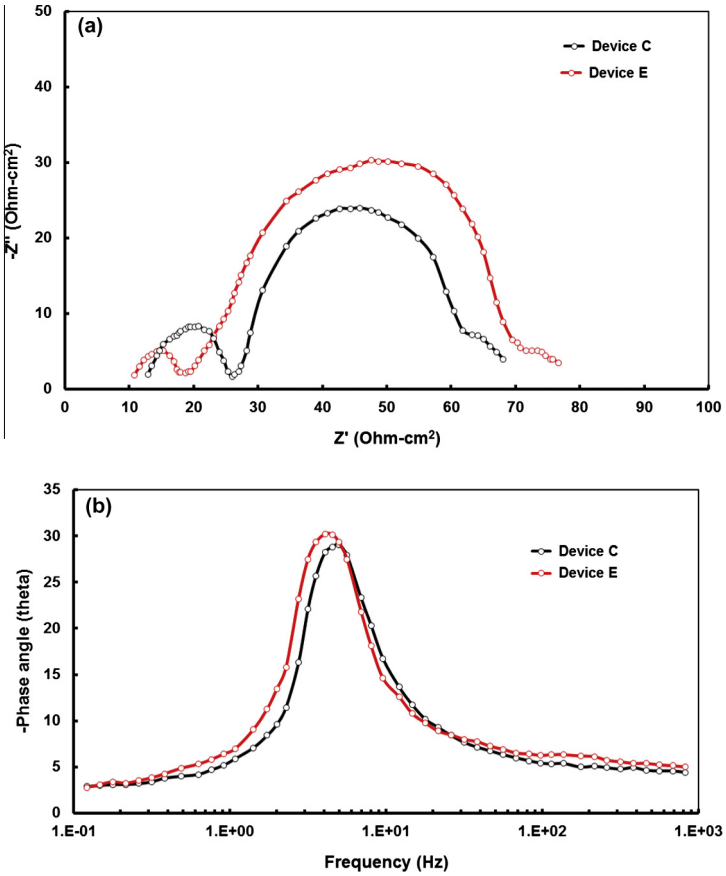

Fig. 8. (a) Nyquist plots (b) Bode phase plots of electrochemical impedance spectra (EIS) for devices **C** and **E**, in dark conditions.

Table 2
Electron transport resistance (R_t), recombination resistance (R_{rec}), electron lifetime (τ_e), electron transfer time (τ_d), and charge collection efficiency (η_{cc}) for devices **C** and **E**.

Device	R_t (Ohm-cm^2)	R_{rec} (Ohm-cm^2)	τ_e (ms)	τ_d (ms)	η_{cc}
C	13.4	35.06	32.64	12.47	0.82
E	8.22	48.45	38.45	6.52	0.88

ate frequency region corresponds to the charge transport resistance at the TiO_2/dye/electrolyte interface and gives information about the chemical capacitance (C_μ) that determines the accumulation of electrons in the TiO_2 CB upon illumination and, therefore, the position of quasi Fermi level of TiO_2 [48]. The chemical capacitance C_μ value for the device with the formic acid treated TiO_2 **ZnP-H_2P** co-sensitized photoanode (device **E**) was found to be higher than that for device **C**. This suggests that the electron density in the formic acid treated TiO_2 is enhanced compared to the pristine TiO_2 under illumination. Moreover, the high value of chemical capacitance C_μ for the formic acid TiO_2 electrode results in a negative shift of the quasi Fermi level of TiO_2, as it was recently reported in literature [49].

The electron transport time (τ_d) of the injected electrons in the TiO_2 film are related with the electron lifetime (τ_e), the charge transport resistance (R_t) and the charge recombination resistance (R_{rec}) according to the following equation [50]

$$\frac{\tau_d}{\tau_e} = \frac{R_t}{R_{rec}} \tag{5}$$

The calculated values of the electron transport time (τ_d) for devices **C** and **E** are listed in Table 2. The electron transport time (τ_d) is a measure of the average time taken by the injected electron to reach the collecting FTO electrode; a faster electron transport time is associated with a higher photocurrent [51]. The reduced charge transport resistance R_t and increased charge recombination resistance R_{rec} values for device **E**, relative to device **C**, lead to a decreased charge transport (τ_d) value and indicate that electrons are collected at the FTO electrode at a faster rate for the formic acid TiO_2 treated photoanode, compared to that for the pristine TiO_2 photoanode. Furthermore, the higher PCE value of device **E** can also be evidently reflected in the charge collection efficiency (η_{cc}) of the device, which calculated by the equation

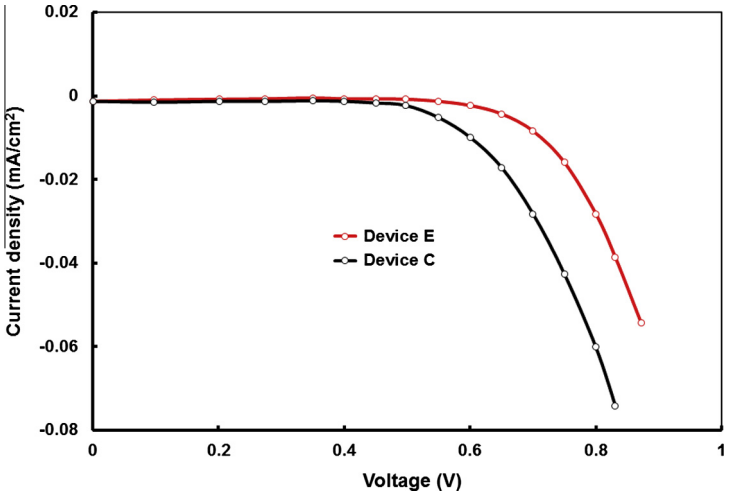

Fig. 9. Dark current–voltage (J–V) characteristics of devices **C** and **E**.

$$\eta_{cc} = \left[1 + \left(\frac{\tau_d}{\tau_e}\right)\right]^{-1} \quad (6)$$

The charge collection efficiency (η_{cc}) values of devices **C** and **E** are listed in Table 2. The higher η_{cc} value for device **E**, compared to device **C**, leads to an enhanced PCE value for the device with the formic acid treated TiO_2 photoanode.

4. Conclusions

In summary, a tertiary arylamine compound (**DC**), with a terminal cyano-acetic group in one of its aryl groups and an unsymmetrical porphyrin dyad of the type Zn[Porph]-L-H_2[Porph] (**ZnP-H_2P**), with a bridging triazine group (L) that is functionalized with a carboxylic acid group of a glycine moiety, were synthesized and used as sensitizers for the fabrication of DSSCs. Photophysical measurements of the two dyes showed broad, strong, and complementary absorptions in their UV–vis spectra, while electrochemistry experiments, and DFT calculations revealed appropriate frontier orbital energy levels for use in DSSCs. The **ZnP-H_2P/DC** and **DC/ZnP-H_2P** co-sensitized solar cells (devices **C** and **D**, respectively) were fabricated, following a stepwise co-sensitization procedure, by immersing the TiO_2 electrode in separate solutions of the dyes in different sequence. The **ZnP-H_2P/DC** co-sensitized solar cell device was found to exhibit a significant improved PCE value (=6.16%), compared to the individually sensitized solar cells based on the **ZnP-H_2P** and **DC** dyes (4.56% and 4.06%, respectively), which is attributed to enhanced photovoltaic parameters (as shown by the corresponding J–V curves). The enhancement of the J_{sc} value of the device is in good agreement with the its enhanced IPCE response, which is ascribed to the improved light harvesting efficiency of the co-sensitizing dyes **ZnP-H_2P/DC** with respect to the individual dyes. Bessho et al. have already reported a PCE of 6.9% for the DSSCs based on the porphyrin dye cosensitized with metal free organic dye [20] and same research group reported a record PCE of 12.3% for similar system [21]. Diau et al. have reported a PCE of 9% for the DSSC based on a porphyrin dye and metal free dye [10]. The PCE of the **ZnP-H_2P/DC** co-sensitized device was further improved up to 7.68% when a formic acid treated TiO_2 photoanode was used (device **E**), which was attributed to the enhanced J_{sc} and V_{oc} values, due to modification of the electronic properties of the TiO_2 CB. Dark current and EIS measurements of device **E** revealed an increased electron transport rate and suppressed electron recombination in the formic acid treated TiO_2 photoanode.

Acknowledgements

Financial support from the European Commission (FP7-REGPOT-2008-1, Project BIOSOLENUTI No. 229927) is greatly acknowledged. This research has been also co-financed by the European Union (European Social Fund–ESF) and Greek national funds through the Operational Program "Education and Lifelong Learning" of the National Strategic Reference Framework (NSRF)-Research Funding Program: Heraklitos II and Operational Program "Education and Lifelong Learning" of the National Strategic Reference Framework (NSRF)-Research Funding Program: THALIS-UOA-MIS 377252. Finally Special Research account of the University of Crete is also acknowledged. KSVG thanks UGC, New Delhi for Senior Research Fellowship. SPS thanks to XII FY CSIR-INTELCOAT (CSC0114) for financial support.

References

[1] B. O'Regan, M. Grätzel, Nature 353 (1991) 737–740.
[2] A. Hagfeldt, G. Boschloo, L. Sun, L. Kloo, H. Pettersson, Chem. Rev. 110 (2010) 6595–6663.
[3] S. Zhang, X. Yang, Y. Numata, L. Han, Energy Environ. Sci. 6 (2013) 1443–1464.
[4] J. Gong, J. Liang, K. Sumathy, Renew. Sustain. Energy Rev. 16 (2012) 5848–5860.
[5] M.-G. Ju, W.Z. Liang, J. Phys. Chem. C 117 (2013) 14899–14911.
[6] A. Islam, H. Sugihara, H. Arakawa, J. Photochem. Photobiol. A 158 (2003) 131–138.
[7] Y. Chiba, A. Islam, Y. Watanabe, R. Komiya, N. Koide, L. Han, Jpn. J. Appl. Phys. 45 (2006) L638–L640.
[8] M.K. Nazeeruddin, P. Pechy, T. Renouard, S.M. Zakeeruddin, R. Hymphry-Baker, P. Comte, P. Liska, L. Cevey, E. Costa, V. Shklover,

L. Spiccia, G.B. Deacon, C.A. Bignozzi, M. Grätzel, J. Am. Chem. Soc. 123 (2001) 1613–1624.
[9] (a) T.W. Hamann, R.A. Jensen, A.B.F. Martinson, H.V. Ryswyk, J.T. Hupp, *Energy Environ. Sci.* 1 (2008) 66–78;
(b) C.Y. Lee, C. She, N.C. Jeong, J.T. Hupp, Chem. Commun. 46 (2010) 6090–6092;
(c) C. Qin, W. Peng, K. Zhang, A. Islam, L. Han, Org. Lett. 10 (2012) 2532–2535;
(d) K. Funabiki, H. Mase, A. Hibino, N. Tanaka, N. Mizuhata, Y. Sakuragi, A. Nakashima, T. Yoshida, Y. Kubota, M. Matsui, *Energy Environ. Sci.* 4 (2011) 2186–2192;
(e) C. Qin, A. Islam, L. Han, Dyes Pigments 94 (2012) 553–560;
(f) T. Bessho, S.M. Zakeeruddin, C.-Y. Yeh, E.W.-G. Diau, M. Grätzel, Angew. Chem. Int. Ed. 49 (2010) 6646–6649.
[10] (a) S.-Q. Fan, C. Kim, B. Fang, K.-X. Liao, G.-J. Yang, C.-J. Li, J.-J. Kim, J. Ko, J. Phys. Chem. C 115 (2011) 7747–7754;
(b) C.-M. Lan, H.-P. Wu, T.-Y. Pan, C.-W. Chang, W.-S. Chao, C.-T. Chen, C.-L. Wang, C.-Y. Lin, E.W.-G. Diau, *Energy Environ. Sci.* 5 (2012) 6460–6464;
(c) D. Kuang, P. Walter, F. Nuesch, S. Kim, J. Ko, P. Comte, S.M. Zakeeruddin, M.K. Nazeeruddin, M. Gratzel, Langmuir 23 (2007) 10906–10909;
(d) Y. Chen, Z. Zeng, C. Li, W. Wang, X. Wang, B. Zhang, New J. Chem. 29 (2005) 773–776;
(e) J.-H. Yum, S.-R. Jang, P. Walter, T. Geiger, F. Nuesch, S. Kim, J. Ko, M. Grätzel, M.K. Nazeeruddin, Chem. Commun. 44 (2007) 4680–4682;
(f) J.N. Clifford, A. Forneli, H. Chen, T. Torres, S. Tan, E. Palomares, J. Mater. Chem. 21 (2011) 1693–1696;
(g) L.H. Nguyen, H.K. Mulmudi, D. Sabba, S.A. Kulkarni, S.K. Batabyal, K. Nonomura, M. Grätzel, S.G. Mhaisalkar, Phys. Chem. Chem. Phys. 14 (2012) 16182–16186;
(h) Y. Shi, R.B.M. Hill, J.H. Yum, A. Dualeh, S. Barlow, M. Grätzel, S.R. Marder, M.K. Nazeeruddin, Angew. Chem. Int. Ed. 56 (2012) 6619–6621;
(i) J. Mao, F. Guo, W. Ying, W. Wu, J. Li, J. Hua, Chem. Asian J. (2012) 982–991;
(j) Z. Ning, Y. Fu, H. Tian, *Energy Environ. Sci.* 3 (2010) 1170–1181;
(k) S. Paek, H. Choi, C. Kim, N. Cho, S. So, K. Song, M.K. Nazeeruddin, J. Ko, Chem. Commun. 47 (2011) 2874–2876;
(l) H. Ozawa, R. Shimizu, H. Arakawa, RSC Adv. 2 (2012) 3198–3200.
[11] (a) L.Y. Han, A. Islam, H. Chen, C. Malapaka, B. Chiranjeevi, S.F. Zhang, X.D. Yang, M. Yanagida, Energy Environ. Sci. 5 (2012) 6057–6060.
[12] R.Y. Ogura, S. Nakane, M. Morooka, M. Orihashi, Y. Suzuki, K. Noda, Appl. Phys. Lett. 94 (2009) 073308–073310.
[13] (a) Y. Chen, Z. Zeng, C. Li, W. Wang, X. Wang, B. Zhang, New J. Chem. 29 (2005) 773–776.
[14] D. Kuang, P. Walter, F. Nuesch, S. Kim, J. Ko, P. Comte, S.M. Zakeeruddin, M.K. Nazeeruddin, M. Grätzel, Langmuir 23 (2007) 10906–10909.
[15] (a) J.J. Cid, J.H. Yum, S.R. Jang, M.K. Nazeeruddin, E.M. Ferrero, E. Palomares, J. Ko, M. Grätzel, T. Torres, Angew. Chem. Int. Ed. 46 (2007) 8358–8362;
(b) J.N. Clifford, A. Forneli, H.J. Chen, T. Torres, S.T. Tan, E. Palomares, J. Mater. Chem. 21 (2011) 1693–1696;
(c) M. Kimura, H. Nomoto, N. Masaki, S. Mori, Angew. Chem. Int. Ed. 51 (2012) 4371–4374.
[16] C.L. Wang, C.M. Lan, S.H. Hong, Y.F. Wang, T.Y. Pan, C.W. Chang, H.H. Kuo, M.Y. Kuo, E.W.G. Diau, C.Y. Lin, Energy Environ. Sci. 5 (2012) 6933–6940.
[17] M.V. Martinez-Diaz, G. de la Torres, T. Torres, Chem. Commun. 46 (2010) 7090–7108.
[18] M. Shrestha, L.P. Si, C.W. Chang, H.S. He, A. Sykes, C.Y. Lin, E.W.-G. Diau, J. Phys. Chem. C 116 (2012) 10451–10460.
[19] C.-M. Lan, H.-P. Wu, T.-Y. Pan, C.-W. Chang, W.-S. Chao, C.-T. Chen, C.-L. Wang, C.-Y. Lin, E.W.-G. Diau, Energy Environ. Sci. 5 (2012) 6460–6464.
[20] T. Bessho, S.M. Zakeeruddin, C.Y. Yeh, E.W.G. Diau, M. Grätzel, Angew. Chem. Int. Ed. 49 (2010) 6646–6649.
[21] A. Yella, H.W. Lee, H.N. Tsao, C.Y. Yi, A.K. Chandiran, M.K. Nazeeruddin, E.W.G. Diau, C.Y. Yeh, S.M. Zakeeruddin, M. Grätzel, Science 334 (2011) 629–634.
[22] (a) J.H. Yum, S.J. Moon, R. Humphry-Baker, P. Walter, T. Geiger, F. Nuesch, M. Grätzel, M.K. Nazeeruddin, Nanotechnology 19 (2008) 424005;
(b) J. Lim, Y.S. Kwon, T. Park, Chem. Commun. 47 (2011) 4147–4149;
(c) Z. Zhang, S.M. Zakeeruddin, B.C. O'Regan, R. Humphry-Baker, M. Grätzel, J. Phys. Chem. B 109 (2005) 21818–21824.
[23] G.E. Zervaki, M.S. Roy, M.K. Panda, P.A. Angaridis, E. Chrissos, G.D. Sharma, A.G. Coutsolelos, Inorg. Chem. 52 (2013) 9813–9825.
[24] K. Ladomenou, T. Lazarides, M.K. Panda, G. Charalambidis, D. Daphnomili, A.G. Coutsolelos, Inorg. Chem. 51 (2012) 10548–10556.
[25] W. Kohn, L.J. Sham, Phys. Rev. 140 (1965) A1133–A1138.
[26] M.J. Frisch, G.W. Trucks, H.B. Schlegel, G.E. Scuseria, M.A. Robb, J.R. Cheeseman, J.A. Montgomery, Jr., T. Vreven, K.N. Kudin, J.C. Burant, J.M. Millam, S.S. Iyengar, J. Tomasi, V. Barone, B. Mennucci, M. Cossi, G. Scalmani, N. Rega, G.A. Petersson, H. Nakatsuji, M. Hada, M. Ehara, K. Toyota, R. Fukuda, J. Hasegawa, M. Ishida, T. Nakajima, Y. Honda, O. Kitao, H. Nakai, M. Klene, X. Li, J.E. Knox, H.P. Hratchian, J.B. Cross, V. Bakken, C. Adamo, J. Jaramillo, R. Gomperts, R.E. Stratmann, O. Yazyev, A.J. Austin, R. Cammi, C. Pomelli, J. Ochterski, P.Y. Ayala, K. Morokuma, G.A. Voth, P. Salvador, J.J. Dannenberg, V.G. Zakrzewski, S. Dapprich, A.D. Daniels, M.C. Strain, O. Farkas, D.K. Malick, A.D. Rabuck, K. Raghavachari, J.B. Foresman, J.V. Ortiz, Q. Cui, A.G. Baboul, S. Clifford, J. Cioslowski, B.B. Stefanov, G. Liu, A. Liashenko, P. Piskorz, I. Komaromi, R.L. Martin, D.J. Fox, T. Keith, M.A. Al-Laham, C.Y. Peng, V. Nanayakkara, M. Challacombe, P.M.W. Gill, B.G. Johnson, W. Chen, M.W. Wong, C. Gonzalez, J.A. Pople, Gaussian 09 (Revision B.01), Gaussian Inc, Wallingford CT 2010.
[27] C.T. Lee, W.T. Yang, R.G. Parr, Phys. Rev. B 37 (1988) 785–789.
[28] A.D. Becke, Phys. Rev. A 38 (1988) 3098–3100.
[29] R. Dennington, T. Keith, J. Millam, GaussView, Version 5, Semichem Inc., Shawnee Mission KS, 2009.
[30] (a) Yasuhiko Shirota, Motoi Kinoshita, Tetsuya Noda, Kenji Okumoto, Takahiro Ohara, J. Am. Chem. Soc. 122 (2000) 11021–11022;
(b) Moon-Sung Kang, Sang Ook Kang, Jaejung Ko, Chulwoo Kim, Hyunbong Choi, Sanghoon Kim, Chul Baik, J. Org. Chem. 73 (2008) 7072–7079.
[31] (a) D. Kim, A. Osuka, Acc. Chem. Res. 37 (2004) 735–745;
(b) N. Aratani, A. Osuka, Y.H. Kim, D.H. Jeong, D. Kim, Angew. Chem. Int. Ed. 39 (2000) 1458–1462;
(c) T.K. Ahn, Z.S. Yoon, I.-W. Hwang, J.K. Lim, H. Rhee, T. Joo, E. Sim, S.K. Kim, N. Aratani, A. Osuka, D. Kim, J. Phys. Chem. B 109 (2005) 11223–11230;
(d) T. Lazarides, G. Charalambidis, A. Vuillamy, M. Reglier, E. Klontzas, G. Froudakis, S. Kuhri, D.M. Guldi, A.G. Coutsolelos, Inorg. Chem. 50 (2011) 8926–8936.
[32] (a) K. Hara, Y. Danoh, C. Kasada, Y. Ohga, A. Shinpo, S. Suga, K. Sayama, Langmuir 20 (2004) 4205–4210;
(b) S. Chang, H. Wang, Y. Hua, Q. Li, X. Xiao, W.K. Wong, W.Y. Wong, X. Zhu, T.J. Chen, Mater. Chem. A 1 (2013) 11553–11558.
[33] Y. Hua, S. Chang, D. Huang, X. Zhou, X. Zhu, J. Zhao, T. Chen, W.-Y. Wong, W.K. Wong, Chem. Mater. 25 (2013) 2146–2153.
[34] (a) H.-P. Wu, Z.-W. Ou, T.-Y. Pan, C.-M. Lan, W.-K. Huang, H.-W. Lee, N.M. Reddy, C.-T. Chen, W.-S. Chao, C.-Y. Yeh, E.W.-G. Diau, Energy Environ. Sci. 5 (2012) 9843–9848;
(b) K.-M. Lee, Y.-C. Hsu, M. Ikegami, T. Miyasaka, K.R.J. Thomas, J.T. Lin, K.-C. Ho, J. Power Sources 196 (2011) 2416–2421.
[35] X.-Z. Guo, Y.-H. Luo, C.-H. Li, D. Qin, D.-M. Li, Q.-B. Meng, Curr. Appl. Phys. 12 (e54e) (2012) e58.
[36] L.H. Nguyen, H.K. Mulmudi, D. Sabba, S.A. Kulkarni, S.K. Batabyal, K. Nonomura, M. Grätzel, S.G. Mhaisalkar, Phys. Chem. Chem. Phys. 14 (2012) 16182–16186.
[37] (a) E. Ronca, M. Pastore, L. Belpassi, F. Tarantelli, F. De Angelis, Energy Environ. Sci. 6 (2013) 183–193;
(b) Y. Duan, N. Fu, Q. Liu, Y. Fang, X. Zhou, J. Zhang, Y. Lin, J. Phys. Chem. C 116 (2012) 8888–8893;
(c) A. Marchioro, A. Dualeh, A. Punzi, M. Grätzel, J.-E. Moser, J. Phys. Chem. C 116 (2012) 26721–26727;
(d) T. Chen, W. Hu, J. Song, G.H. Guai, C.M. Li, Adv. Funct. Mater. 22 (2012) 5245–5250;
(e) Z. Lan, J. Wu, J. Lin, M. Huang, J. Mater. Chem. 21 (2011) 15552–15557.
[38] (a) L. Meng, C. Li, Nanosci. Nanotechnol. Lett. 3 (2011) 181–185;
(b) M.S. Goes, E. Joanni, E.C. Muniz, R. Savu, T.R. Habeck, P.R. Bueno, F. Fabregat-Santiago, J. Phys. Chem. C 116 (2012) 12415–12421;
(c) A. Burke, S. Ito, H. Snaith, U. Bach, J. Kwiatkowski, M. Grätzel, Nano Lett. 8 (2008) 977–981.
[39] J.W. Ondersma, T.W. Hamann, Coord. Chem. Rev. 257 (2013) 1533–1543.
[40] (a) E. Palomares, J.N. Clifford, S.A. Haque, T. Lutz, J.R. Durrant, J. Am. Chem. Soc. 125 (2002) 475–482;
(b) C.-S. Chou, F.-C. Chou, J.-Y. Kang, Powder Technol. 215 (2012) 38–45;
(c) S. Wu, X. Gao, M. Qin, J.-M. Liu, S. Hu, Appl. Phys. Lett. 99 (2011) 042106;

(d) Q. Hu, C. Wu, L. Cao, B. Chi, J. Pu, L. Jian, J. Power Sources 226 (2013) 8–15.
[41] (a) K.-H. Park, E.M. Jin, H.B. Gu, S.E. Shim, C.K. Hong, Mater. Lett. 63 (2009) 2208–2211;
(b) G.H. Guai, Q.L. Song, Z.S. Lu, C.M. Ng, C.M. Li, Renew. Energy 51 (2013) 29–35;
(c) S. Hao, J. Wu, L. Fan, Y. Huang, J. Lin, Y. Wei, Sol. Energy 76 (2004) 745–750.
[42] (a) X.-T. Zhang, H.-W. Liu, T. Taguchi, Q.-B. Meng, O. Sato, A. Fujishima, Sol. Energy Mater. Sol. Cells 81 (2004) 197–203;
(b) T. Peng, K. Fan, D. Zhao, J. Chen, J. Phys. Chem. C 114 (2010) 22346–22351;
(c) E. Palomares, J.N. Clifford, S.A. Haque, T. Lutz, J.R. Durrant, J. Am. Chem. Soc. 125 (2002) 475–482;
(d) A. Kay, M. Grätzel, Chem. Mater. 14 (2002) 2930–2935;
(e) G.A. Spyroulias, A.G. Coutsolelos, Polyhedron 14 (1995) 2483–2490;
(f) L. Grinis, S. Kotlyar, S. Ruhle, J. Grinblat, A. Zaban, Adv. Funct. Mater. 20 (2010) 282–288;
(g) G. Chen, X. Ning, B. Park, G.-J. Boons, B. Xu, Langmuir 25 (2009) 2860–2864;
(h) K.-W. Wu, A. Tedla, Y.-T. Mu, Y.J. Tai, Mater. Chem. A 1 (2013) 12137–12143.
[43] M.-C. Chen, Y.-S. Chiou, J.-M. Chiu, A. Tedla, Y.J. Tai, Mater. Chem. A 1 (2013) 3680–3687.
[44] B.C. O'Regan, J.R. Durrant, Acc. Chem. Res. 42 (2009) 1799–1808.
[45] L.A. Lyon, J.T.J. Hupp, Phys. Chem. B 103 (1999) 4623–4628.
[46] (a) R. Kern, R. Sastrawan, J. Ferber, R. Stangl, J. Luther, Electrochim. Acta 47 (2002) 4213–4225;
(b) M.J. Tornaritis, A.G. Coutsolelos, Polymer 33 (1992) 1771–1772;
(c) L. Han, N. Koide, Y. Chiba, T. Mitate, Appl. Phys. Lett. 84 (2004) 2433–2435;
(d) Q. Wang, J.-E. Moser, M. Grätzel, J. Phys. Chem. B 109 (2005) 14945–14953.
[47] (a) H. Tian, L. Hu, C. Zhang, W. Liu, Y. Huang, L. Mo, L. Guo, J. Sheng, S. Dai, J. Phys. Chem. C 114 (2010) 1627–1632;
(b) S.K. Park, C. Kim, J.H. Kim, J.Y. Bae, Y.S. Han, Curr. Appl. Phys. 11 (2011) S131–S135.
[48] (a) J. Bisquert, F.F. Santiago, I.N.M. Sero, G.G. Belmonte, S. Gimenez, J. Phys. Chem. C 113 (2009) 17278–17290;
(b) A. Hagfeldt, G. Boschloo, L. Sun, L. Kloo, H. Pettersson, Chem. Rev. 110 (2010) 6595–6663.
[49] V. Saxena, P. Veerender, A. Gusain, P. Jha, J. Singh, S.P. Koiry, P.V. Varde, A.K. Chauhan, D.K. Aswal, S.K. Gupta, Org. Electron. doi.org/10.1016/j.orgel.2013.07.020.
[50] J. van de Langemaat, A.J. Frank, J. Phys. Chem. B 104 (2000) 4292–4294.
[51] M. Adachi, M. Sakamoto, J.T. Jiu, Y. Ogata, S. Isoda, J. Phys. Chem. B 110 (2006) 13872–13880.